PERGAMON

Computers and Structures 76 (2000) 379–397

Computers & Structures

www.elsevier.com/locate/compstruc

Finite element modeling of the resin transfer molding process based on homogenization techniques

Z. Dimitrovová [a,*], L. Faria [b]

[a] IDMEC, Instituto Superior Técnico, Av. Rovisco Pais 1, 1096, Lisboa, Portugal
[b] Departamento de Engenharia Mecânica, Instituto Superior Técnico, Av. Rovisco Pais 1, 1096, Lisboa, Portugal

Abstract

New aspects are introduced into the numerical simulation of the mold filling phase of the Resin Transfer Molding process of composites manufacturing. The problem formulation is based on homogenization techniques. The well-known analogy with the micro-level analysis is mentioned and the permeability determination in the case of single and double porosity is shown. Regarding the macro-level analysis, the analogous problem, which has not been used earlier for such purpose, is discussed. The determination of a resin front position in orthotropic and multiple-layer preforms is addressed. Results obtained by the finite element code ANSYS are compared with previous works.

Keywords: Resin transfer molding; Numerical simulation; Finite elements; Homogenization techniques; Orthotropic preforms; Multiple-layer preforms

1. Introduction

The Resin Transfer Molding (RTM) process has recently become one of the most important processes of fiber reinforced composites manufacturing. The process consists of three phases: an arrangement of fiber mats in a mold cavity, a mold filling by a polymeric resin and a curing phase. The last two phases may be considered as independent, since the characteristics of the RTM process (resin properties, applied pressure or flow rate at injection gates, applied temperature, location of injection gates and air vents, etc.) are usually chosen in such a way that the curing phase starts after the mold filling phase is completed.

The main objective in the numerical simulation of the mold filling phase is to determine the progression of the resin front position and the evolution of the pressure and the temperature distribution. The numerical simulation should also discover hard-to-fill regions and regions of possible void formation. Advanced simulations should permit an optimization of the injection gates and air vents locations, of the mold geometries and of other RTM process characteristics mainly with respect to the mold filling time, which is one of the principal cost factors of the full RTM process.

Due to the large number of fibers and very low ratio of their characteristic cross-sectional size to the size of the mold, direct numerical solution of the filling-phase problem (accounting for all fiber geometry details) is almost impossible. Homogenization techniques are often used in order to reformulate the original problem in terms of the micro-level (local) and the macro-level (global, effective) analyses.

Sometimes, it is possible to neglect the temperature influence. Then, for resins that usually come into account, the resin flow can be viewed as slow flow

* Corresponding author.
E-mail address: zdimitro@dem.ist.utl.pt (Z. Dimitrovová).

0045-7949/00/$ - see front matter
PII: S0045-7949(99)00174-1

(low Reynolds number flow) of an incompressible isotropic Newtonian liquid with high viscosity and constant properties. In this case the micro-level and macro-level analyses have forms that allow finding problems analogous with them, which are included in many general-purpose commercial finite element (FE) codes, e.g. in ANSYS or ABAQUS. It should be remarked that ABAQUS allows for, under some restrictions, direct solution of the macro-level problem (coupled pore fluid flow and stress analysis), as already mentioned in Ref. [1]. This paper is mainly devoted to the implementation of the RTM filling phase in ANSYS and ABAQUS is only briefly commented.

Most of the FE codes suited for the RTM filling-phase simulation deal only with the global analysis, where the progression of the resin front is based on the control volume (CV) approach [2,3]. Another recent idea, which has been proposed in Ref. [4], exploits for this purpose non-conforming FE. These approaches are not included in the general-purpose commercial FE codes, such as ANSYS (see [5–7]) or ABAQUS (see [8–10]). It must be emphasized that in the analogous problem for the macro-level analysis, discussed in this paper, the progression of the resin front is resolved differently than in FE/CV and non-conforming FE approaches, exploiting at this point the approach utilized in the pore fluid flow analysis in ABAQUS.

The paper is organized in the following way. In Section 2 the basic facts required from homogenization techniques in view of the RTM filling phase are briefly summarized. Section 3 is devoted to the micro-level analysis and Section 4 to the macro-level analysis. Namely, in Section 3 the well-known analogy is mentioned, some results of the permeability tensor (which determination is the main objective of the micro-level analysis) are shown and compared with the results previously published. Numerical stability of the results is discussed and comments to the permeability determination in the case of double porosity (see [11–13]) are added. In Section 4.1 the analogous problem for the macro-level analysis, which (according to the authors' knowledge) has so far not been used for such purpose, is presented. In Section 4.2 the numerical stability of the results is discussed and the advantages and disadvantages of the proposed approach with respect to the FE/CV and the non-conforming FE approaches are summarized. In Section 4.3 two examples taken from Ref. [4] and a study of an orthotropic preform are presented in order to verify the proposed approach. Section 4.4 introduces an approach to the determination of a non-uniform resin front in multiple-layer preforms. The paper is concluded in Section 5.

The first contribution of this paper lies in the summary of the one of the simplest approaches to the *permeability determination*. Regarding the macro-level analysis, a *different resolution of the resin front progression* bringing several advantages, however, also some disadvantages with respect to the FE/CV and non-conforming FE approaches is the second contribution of this paper. The third contribution is in the introduction of a different conception in the *multiple-layer preform analysis* than in Refs. [14,15]. In this paper the correctness of the thickness-averaged permeability is justified and the calculation of the non-uniform front characteristics is proposed in a different way. Analytical predictions are in better coincidence, than the ones presented in Refs. [14,15], with the numerical results of specimens accounting for different layer properties. It is also concluded that when the analytical predictions of the non-uniform front are required, distinction between unsaturated and saturated permeability (proposed in Ref. [16]) is not necessary.

2. Homogenization techniques

At first, the original problem is formulated. Due to the simplifying assumptions specified in Section 1, governing equations will be related only to the resin flow and the terms corresponding to the chemical reactions and heat transfer will be disregarded. As usual, the influence of the surface tension and the air pressure on the resin front is neglected. Together with the other features (slow flow of incompressible isotropic Newtonian liquid with constant properties) the conservation of mass (the continuity equation) and the conservation of momentum (the equilibrium equation) can be written as [17]:

$$\nabla \cdot \mathbf{v} = 0 \text{ and } \rho \frac{\partial \mathbf{v}}{\partial t} = -\nabla p + \mu \Delta \mathbf{v} + \mathbf{F}, \tag{1}$$

where $\mathbf{v}$, t, p, $\mathbf{F}$ stand for the velocity vector, time, pressure and the volumetric force vector, respectively; ρ and μ are the resin density and the coefficient of the resin viscosity. As usual $\nabla = \{\partial/\partial x_1, \partial/\partial x_2, \partial/\partial x_3\}$, $\mathbf{x}$ is the spatial variable, $\Delta = \nabla \cdot \nabla$ and "$\cdot$" stands for the tensor multiplication (with one repeated index if indicial notation is used). It may be remarked that the time derivative in Eq. (1) is partial. Fibers are assumed impermeable, rigid, with perfectly fixed location and since the air influence was already neglected, the boundary conditions take simple forms [17]:

at the resin front: $\partial f/\partial t + \mathbf{v} \cdot \nabla f = 0$, $\sigma \cdot \mathbf{n} = \mathbf{0}$,

at the mold walls and the fiber boundary: $\mathbf{v} = \mathbf{0}$,

at the injection gates: $\mathbf{v} = \mathbf{v}_0$ or $p = p_0$, (2)

where $\mathbf{n}$ is the unit normal vector to the corresponding surface, $\boldsymbol{\sigma}$ stands for the stress tensor and subscript 0 refers to the imposed values. The function $f(\mathbf{x}(t), t) = 0$ describes the moving front position. The first condition at the resin front (simply written as $\mathrm{d}f/\mathrm{d}t = 0$) is known as *the free boundary condition* and the condition $\mathbf{v} = \mathbf{0}$ is called *the no-slip condition* [17].

As already mentioned in Section 1, direct numerical solution of the problem (1)–(2), with all fiber geometry details included, is almost impossible. In order to formulate the micro- and macro-level problems equivalent to (1)–(2), either asymptotic expansion (see [12, 18–20]) or local averaging (see [20]) methods of homogenization techniques can be used. When the geometry of the preforms is periodic, under the assumptions already adopted, the two methods yield similar formulations. In periodic media, a basic cell ϑ can be introduced as the smallest part of the medium, which can generate the full one by a periodic repetition, and the averaging operator, $\langle\cdot\rangle$, defined as $\langle\cdot\rangle = \frac{1}{|\vartheta|}\int_{\vartheta}\cdot\,\mathrm{d}\vartheta$ ($|\vartheta|$ is the volume of the basic cell), can be defined.

It turns out, that the macro-level problem is in fact the well-known Darcy's law for incompressible flows through porous media (determined also empirically, see [21]). If the volumetric forces are neglected, it is usually written in the form:

$$\nabla\cdot\mathbf{v}^{\mathrm{D}} = 0 \text{ and } \mathbf{v}^{\mathrm{D}} = -\frac{\mathbf{K}}{\boldsymbol{\mu}}\cdot\nabla P, \tag{3}$$

where the first relation is the *macroscopic equation* of the homogenization theory corresponding to *the continuity equation inside the saturated regions*, $\mathbf{v}^{\mathrm{D}}$ is known as the vector of the Darcean velocity and P is the macroscopic (global) pressure; $\mathbf{K}$ stands for the permeability tensor and has to be determined from a micro-level problem. Both, $\mathbf{v}^{\mathrm{D}}$ and P, are obtained from the microscopic (local) values, $\mathbf{v}$ and p, by averaging, i.e. $\mathbf{v}^{\mathrm{D}} = \langle\boldsymbol{v}\rangle$ and $P = \langle p\rangle$.

The boundary conditions for the macro-level problem are:

$$\text{at the resin front: } \partial f/\partial t + \left(\mathbf{v}^{\mathrm{D}}\cdot\nabla f\right)/\phi = 0,\ P = 0,$$

$$\text{at the mold walls: } \partial P/\partial n = 0,$$

$$\text{at the injection gates: } \mathbf{v}^{\mathrm{D}} = \langle\langle\mathbf{v}_0\rangle\rangle \quad \text{or} \quad P = \langle\langle P_0\rangle\rangle, \tag{4}$$

where ϕ is the porosity and $\langle\langle\cdot\rangle\rangle$ stands for the area average at the injection gates, which is in fact not necessary, since no fibers will be present in this region. Actually, the no-slip condition $\mathbf{v}^{\mathrm{D}} = \mathbf{0}$ should hold at the mold walls. Taking into account the continuity equation, $\mathbf{v}^{\mathrm{D}} = \mathbf{0}$ is usually simplified to $\partial P/\partial n = 0$, but exact satisfaction of $\mathbf{v}^{\mathrm{D}} = \mathbf{0}$ is not ensured by $\partial P/\partial n = 0$. The error is negligible only when $\mathbf{K}/\mu$ is small.

The micro-level problem resulting from the asymptotic expansion method is formulated e.g. in Refs. [12,18–20]. Steady-state form (Stokes flow) of (1)–(2) is taken as a starting point, into which asymptotic expansion of the velocity vector and pressure is substituted. The first non-zero term from the asymptotic expansion of the velocity vector (for the sake of simplicity with the square of the small parameter included), $\mathbf{v}^{(0)}$, is given by (summation convention is adopted):

$$\mathbf{v}^{(0)} = \frac{\boldsymbol{\chi}^m}{\mu}\left(F_m - \frac{\partial p^{(0)}}{\partial x_m}\right),$$

where $\boldsymbol{\chi}^m$ is a characteristic solution of the *microscopic equation* of the homogenization theory, fulfilling $K_{\mathrm{im}} = \langle\chi_i^m\rangle$. $p^{(0)}$ is the first non-zero term from the pressure expansion and $\mathbf{v}^{\mathrm{D}} = \langle\boldsymbol{v}^{(0)}\rangle$ and $P = \langle p^{(0)}\rangle$. $\boldsymbol{\chi}^m$ is, in fact, the velocity vector related to Stokes flow of the unit-viscosity liquid in the (fully filled) basic cell, if either negative unit macro-pressure gradient or positive unit uniform volume force in direction m is applied on the basic cell. Periodicity boundary conditions must be imposed on χ^m components and on the pressure. Although, when the pressure gradient is applied, the periodicity must be satisfied by the boundary pressure reduced by the value corresponding to the imposed gradient. The main advantage of the micro-level problem in this case is that the problem is linear and the permeability tensor depends only on *the geometry of the fiber mats*.

Obviously, the geometry of the preforms is not strictly periodic, but it is always possible to take typical cells from different regions, calculate the permeability tensor for them and allow the permeability to vary with respect to the macroscopic spatial coordinate.

Nowadays, the numerical calculation of the permeability tensor is still not common, mainly due to the complicated geometry of the fiber mats, therefore values obtained from experimental measurements are usually introduced into the macro-level problem.

It should be emphasized that the typical specimens are relatively thin, allowing the macro-level problem to be stated only on a two-dimensional surface. However, preforms consist of various (macroscopically homogeneous) layers, stacked together, whose directional properties are usually very different. In order to restrict the analysis to a two-dimensional surface, another homogenization step must be done in the transversal (thickness) direction. This problem is addressed in Section 4.4.

3. Micro-level analysis: analogous problem and numerical results

Since Stokes flow in a (fully saturated) basic cell has to be solved, the well-known analogy with incompressible elasticity can be used (see e.g. [22]). Thus the velocity vector from the original problem is related to the displacement vector in the analogous problem. Continuity equation (incompressibility) can be satisfied (with sufficient exactness) by introduction of the Poisson's ratio of the related elastic material very close to 0.5. Regarding the input of the analogous problem to FE codes, it is more convenient to prescribe the unit uniform volume force (as the macroload) than the pressure gradient. Periodicity conditions can only be imposed on the boundary displacements, since due to the variational formulation of the problem, they enforce the periodicity of the boundary pressure. Among disadvantages of ANSYS, with respect to the solution of the analogous problem, can be included:

- The hybrid formulation is not available for linear elastic elements and thus the pressure is calculated from the stress components at Gauss points. Detailed discussion of the problems, which can appear in this case, namely the mesh locking and the necessity of satisfaction of the Babuska–Brezzi condition, can be found in Ref. [22].
- The generalized plane strain option is not available for two-dimensional basic cells, but, since a rigid fiber cut must be present in the cell, assumptions of either generalized plane strain or plane strain yield the same results.

From several advantages of ANSYS, it should be especially mentioned:

- Availability of the macro "PERI" allowing for direct introduction of the periodicity boundary conditions, see [5].
- Powerful preprocessor, very well organized for an interactive usage, allowing for an introduction of complicated geometries and for an easy creation of a FE mesh.
- ANSYS Parametric Design Language permitting an automatization of the preprocessing.
- No need of a special subroutine calculating averaged values. The command "ETABLE" and commands for operations can be used for this purpose, see [6].

Other possibility of calculation of the average value in the basic cell can be mentioned. Exploiting the continuity equation in the part of the cell occupied by the resin, ϑ_r, and the no-slip condition on the resin-fiber interface, S_{rf}, it holds (in terms of the original problem):

$$|\vartheta|\langle v_i\rangle = \int_{\vartheta_r} v_i \,\mathrm{d}\mathbf{x} = \int_{\vartheta_r} v_k \frac{\partial x_i}{\partial x_k}\,\mathrm{d}\boldsymbol{x} = -\int_{\vartheta_r} \frac{\partial v_k}{\partial x_k} x_i \,\mathrm{d}\mathbf{x} + \int_{S_{rf}} v_k n_k x_i \,\mathrm{d}\boldsymbol{S} + \int_{\partial\vartheta} v_k n_k x_i \,\mathrm{d}\boldsymbol{S} = \int_{\partial\vartheta} v_k n_k x_i \,\mathrm{d}\boldsymbol{S},$$

where $\partial\vartheta$ is the boundary of ϑ.

As a two-dimensional example, permeability values for a perpendicular flow across aligned circular fibers with in-line arrangement were calculated. This is a well-known example whose results are published e.g. in Ref. [12] — calculation using FE, in Ref. [20] — calculation using finite differences, in Ref. [11] — calculation using boundary elements, etc. This simple case also has an analytical solution as demonstrated in Ref. [23]. Permeability results are not presented here, since they can be found in the above references. Only the graph of the numerical sensitivity of the dimensionless permeability on the Poisson's ratio of the related elastic material is plotted in Fig. 1. The particular chosen case is the one, where the dimensionless (with respect to the cell dimension) fiber radius is 0.25 and the permeability values are divided by the full area of the cell, to get a dimensionless form. It is seen that the numerical stability of the permeability results is very good.

Relating to the absence of the hybrid formulation for linear elastic elements in ANSYS, it can be remarked that in the studied cases small variations in the pressure values but no variations in the velocity (displacement) values for different Poisson's ratios were obtained. Since only the velocity (displacement) values are required for the permeability determination, this ANSYS disadvantage does not influence the intended results. Validation of the results by ABAQUS, where the hybrid formulation is available [9,10], was also performed.

Some velocity (displacement) components in the opposite direction than applied volumetric forces were found in the example described above, demonstrating the existence of the recirculation regions, as already mentioned in Ref. [11]. The values are

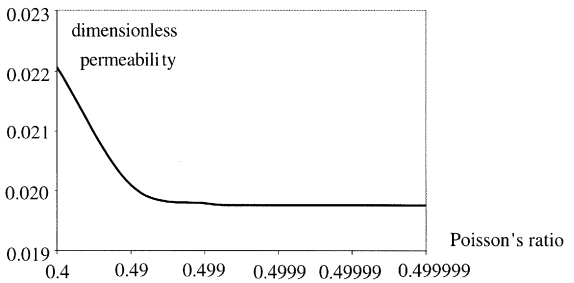

Fig. 1. Numerical sensitivity of the dimensionless permeability on the Poisson's ratio of the related elastic material for perpendicular flow across aligned circular fiber (dimensionless radius of the fiber is 0.25).

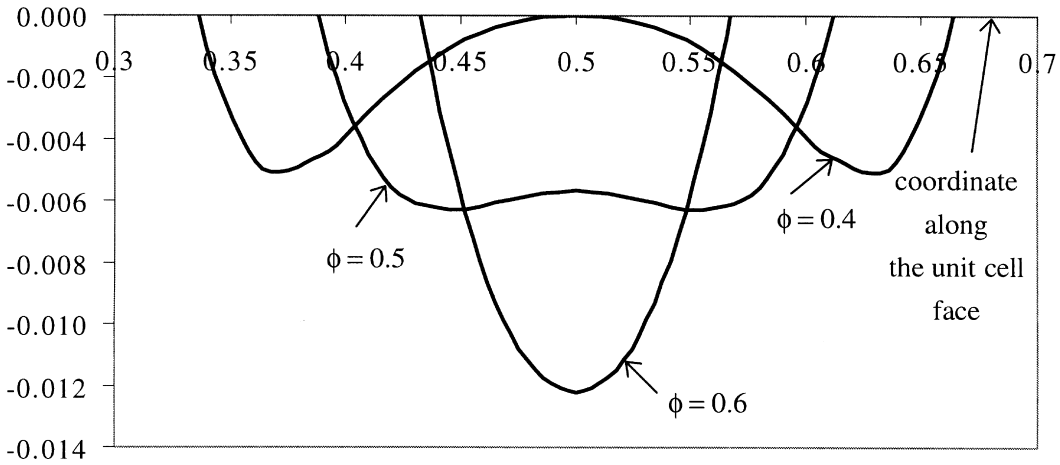

Fig. 2. Velocity values (dimensionless with respect to the corresponding maximum value along the face) on a part of the basic cell face, justifying the existence of the recirculation regions (the assumed porosities are $\phi = \{0.4, 0.5, 0.6\}$).

plotted in a dimensionless form along the basic cell face in Fig. 2 for porosities $\phi = \{0.4, 0.5, 0.6\}$.

When the problem of double porosity (if fibers are in fact fiber-tows consisting of several fibrils, see [11–13]) is addressed, in some cases it is not necessary to solve the macro-level problem in two levels, but *the cell-averaged permeability* can be directly introduced into the macro-level problem. In order to calculate it, all the single fibrils constituting the fiber-tows have to be modeled in the basic cell. Due to the ANSYS powerful preprocessor, this is a straightforward problem and results are easily obtainable from the linear analogous problem as before. Let the perpendicular flow across aligned circular fiber-tows with in-line arrangement be assumed again. FE mesh in the basic cell for the inter-tow porosity 0.5 (when assuming the fiber-tows as full), the intra-tow porosity 0.4 (within the fiber-tow) and number of fibrils 21 is presented in Fig. 3. The coincidence of the results with the ones published in Ref. [11] was verified.

It can be concluded that in ANSYS the components of the permeability tensor are obtainable directly and quickly by a linear and numerically stable calculation. The results depend only on the geometry of the fiber mats. Recirculation regions can be detected in addition to these results.

4. Macro-level analysis

4.1. Analogous problem

Problem (3) with boundary conditions (4) can be reformulated. The continuity equation $\nabla \cdot \mathbf{v}^{\mathrm{D}} = 0$, valid only inside the saturated regions as already mentioned in Section 2, can be extended to a more general form, valid inside the full mold domain. Such a form (derived e.g. in Ref. [10] in a more general context) accounts directly for the transient effects and allows for a direct determination of the resin front position at each time stage. Then the reformulated Darcy's analysis resembles the heat transfer analysis [24]. The governing equations are the following:

$$\gamma\left(\phi(\mathbf{x})\frac{\partial}{\partial t}s(\mathbf{x},t) + \nabla\cdot\mathbf{v}^{\mathrm{D}}(\mathbf{x},t)\right) = 0, \quad \text{(Darcy's analysis)}$$

$$\rho_c\frac{\partial}{\partial t}U(\mathbf{x},t) + \nabla\cdot\mathbf{q}(\mathbf{x},t) = 0, \quad \text{(Heat transfer analysis)}$$

$$\mathbf{v}^{\mathrm{D}}(\mathbf{x},t) = -\frac{\mathbf{K}(\mathbf{x})}{\mu}\cdot\nabla P(\mathbf{x},t) \quad \text{(Darcy's analysis)},$$

$$\mathbf{q}(\mathbf{x},t) = -\mathbf{T}(\mathbf{x})\cdot\nabla\Theta(\mathbf{x},t) \quad \text{(Heat transfer analysis)}. \tag{5}$$

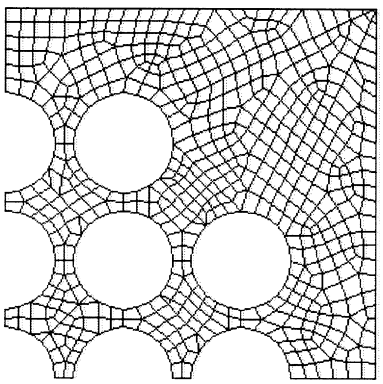

Fig. 3. FE mesh in the basic cell used in the calculation of the cell-averaged permeability for perpendicular flow (the inter-tow porosity is 0.5, intra-tow porosity is 0.4 and the number of fibrils is 21).

The fields not yet defined in Darcy's analysis are: γ and s, denoting the resin specific weight and the saturation in the porous medium. Relating to the analogous problem: ρ_c, U, $\mathbf{q}$, $\mathbf{T}$ and Θ stand for the density, internal energy (the heat content per unit mass), heat flux vector, thermal conductivity tensor and the temperature, respectively.

In this case the boundary conditions (4) do not have to be reformulated, only the free boundary condition can be omitted. It may be remarked that the free boundary condition is also not utilized directly in the other (FE/CV [2,3] and non-conforming FE [4]) approaches.

The continuity equation in (5), in fact, expresses the equation of the moving front, $f(\mathbf{x}(t), t) = 0$. In the fully saturated regions saturation reaches its limit, value 1, and becomes time independent, giving the continuity equation as $\nabla \cdot \mathbf{v}^{\mathrm{D}} = 0$. At the resin front both terms in the continuity equation in (5) tend to infinity. Let us assume a one-dimensional case with one inlet. Time derivation of the saturation (under the assumption of increasing saturated length $L(t)$) obviously tends to $-\delta(L(t))$, where δ is the Dirac function. The only "non-zero" spatial derivative of the velocity is $\delta(x(t))$, marking the position $x(t)$, where there is a discontinuity in the velocity field. Thus

$$f(x(t), t) = x(t) - L(t) = 0 \tag{6}$$

is the resin front equation in one-dimensional case. Roughly speaking for the general case, the drop in saturation must be in the place where there is a drop in the normal to the front component of $\mathbf{v}^{\mathrm{D}}$.

Going back to the problem (5), let us assume $\rho_c = 1$ in the heat transfer and $\gamma = 1$ in the Darcy's analyses. Then Table 1 states the possible analogy (γ was introduced into Darcy's analysis only in order to obtain similar relations between the corresponding units).

Since the saturation, s, is restricted to the interval [0, 1], the same kind of restriction must be ensured in the analogous (heat transfer) problem, thus U must always belong to the interval $[0, \phi]$. In order to explain how to do it, a *fictitious medium* has to be introduced, for which a special kind of heat transfer properties will be defined and for which some equivalents of the terms "porosity" and "saturation" should be introduced. However, for the sake of simplicity, these terms will be kept, but when related to the heat transfer analysis they will be written in quotes. Also the notation ϕ will be used in the analogous problem with its "original" meaning.

Furthermore, *a front region with finite width* has to be defined.

The relation (see e.g. [10])

$$\frac{\partial}{\partial t} U(\mathbf{x}, t) = c(\mathbf{x}, t) \frac{\partial}{\partial t} \Theta(\mathbf{x}, t), \text{ where } c(\mathbf{x}, t) = \frac{\mathrm{d}}{\mathrm{d}\Theta} U\big(\Theta(\mathbf{x}, t)\big)$$

will be exploited (c being the specific heat) in order to define the fictitious medium. Under assumption of linear "heat gaining", c is piece-wise constant with two different values, non-zero ($c = c_0$) and zero ($c = 0$) defining two regions like that. They are: the region where the fictitious medium is not yet "fully saturated" (including the front region, where the medium already started to gain heat) and the region where the medium is already "fully saturated". In order to model such situation, an initial temperature, Θ_i, must be introduced in the fictitious medium, and a temperature, Θ_{s}, that will correspond to the "saturated state" has to be stated. Both values cannot vary throughout the medium, since they cannot originate some additional heat fluxes; only $c_0(\mathbf{x})$ can reflect the variation of the "porosity" $\phi(\mathbf{x})$, meaning that the regions with higher "porosities" gain heat faster. It holds:

$$\phi(\mathbf{x}) = (\Theta_{\mathrm{s}} - \Theta_i) c_0(\mathbf{x}) \tag{7}$$

and the front region is characterized by $\Theta \in (\Theta_i, \Theta_{\mathrm{s}}]$.

Since the temperature in this analogous problem is related to the pressure from the original analysis, introduction of Θ_i could be viewed as some initial pressure. In this context one could refer to the pore fluid flow analysis in ABAQUS [8,10], where it is moreover necessary to introduce some initial saturation (actually the minimum allowed is 0.01, which is quite high). In the proposed approach this is not needed and it was verified that the results are basically independent on

Table 1
Correspondence between fields in the heat transfer and Darcy's analyses

Field in Darcy's analysis	Unit	Field in heat transfer analysis	Unit
$\gamma\phi s$ ($\gamma = 1$)	$[\mathrm{ML}^{-3}]$	$\rho_c U$ ($\rho_c = 1$)	$[\mathrm{JL}^{-3}]$
$\gamma \mathbf{v}^{\mathrm{D}}$	$[\mathrm{ML}^{-2}\mathrm{T}^{-1}]$	$\mathbf{q}$	$[\mathrm{JL}^{-2}\mathrm{T}^{-1}]$
$\gamma \mathbf{K}/\mu$	[T]	$\mathbf{T}$	$[\mathrm{JL}^{-1}\mathrm{T}^{-1}\,\theta^{-1}]$
P	$[\mathrm{ML}^{-1}\mathrm{T}^{-2}]$	Θ	$[\theta]$

the choice of c_0, in other words independent on the choice of Θ_i and Θ_s. It is only necessary to adjust c_0 in order to reflect as much as possible the original problem.

It turns out that c_0 is related directly to the width of the heat flux front region as can be shown in a rough calculation. The heat flux can be taken as constant, q_0, in the region close to the front at time $t = t_0$, and linear inside the front region, see Fig. 4. Let us denote by l the heat flux front width in the normal direction to the front and for the corresponding component of $\mathbf{T}$ let us use T_n. Assuming this problem as one-dimensional, one gets:

$$\Theta_s - \Theta_i = \frac{q_0 l}{2T_n}$$

and together with (7):

$$c_0 = \frac{2T_n\phi}{lq_0}. \tag{8}$$

If some appropriate value of l is chosen, relation (8) can be used to obtain c_0 estimate. It does not mean that by adopting a suitable front width l, c_0 has to vary in accordance with q_0, which is anyway mostly unknown. Roughly speaking, a low c_0 yields a large width, which distorts the results of the original problem (resin front is badly defined), but on the other hand a low c_0 usually ensures faster convergence of the transient analysis. For very high c_0 one should be aware of the numerical stability of the results and sometimes of slow convergence.

After some c_0 estimate was taken, the governing equation to be solved in the fictitious medium is ($\rho_c = 1$):

$$c\frac{\partial}{\partial t}\Theta(\mathbf{x}, t) - \nabla \cdot \big(\mathbf{T}(\mathbf{x}) \cdot \nabla\Theta(\mathbf{x}, t)\big) = 0.$$

It can be reminded (see Table 1), that relating to the Darcy's analysis ($\gamma = 1$), the thermal conductivity tensor $\mathbf{T}$ corresponds to the ratio of the permeability tensor over the viscosity $\mathbf{K}/\mu$ and the temperature, Θ, to the pressure, P. In SI units, the ratio $\mathbf{K}/\mu$ has usually low value, on the other hand, pressure values are quite high. This fact could influence the numerical stability of the results. One can multiply $\mathbf{K}/\mu$ by 10^m with some suitable m, then the c_0 estimate should be done for $(\mathbf{K}/\mu)\ 10^m$ and the resulting pressure has to be multiplied by 10^m.

The analogy described in this section performs well. ANSYS time integration in the analogous problem is unconditionally stable, the transient integration parameter, β, can vary within [1/2, 1], see [7]. The important thing is that $\beta = 1/2$, defining the central difference method, is allowed (it is default). This high accuracy of the time integration is necessary in dealing with the

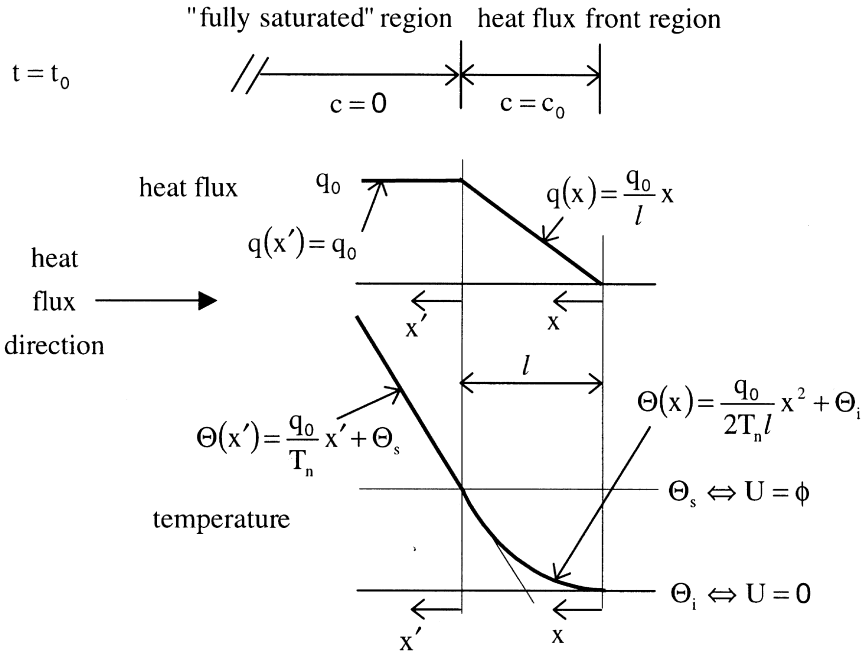

Fig. 4. Simplified assumptions about the heat flux and the temperature distribution in the front region, allowing the estimation of the value c_0.

discontinuity in the time derivative of the internal energy. In ABAQUS such choice is not possible, only backward difference algorithm ($\beta = 1$) is available in the analogous analysis, see [10], making the results highly unreliable (see Section 4.2).

4.2. The numerical stability of the analogous problem results

In order to examine the numerical stability and reliability of the analogous problem results, simple one-dimensional examples, permitting an analytical solution, are examined.

A specimen with the total length $D = 0.3$ m, $\mathrm{K}/\mu = 25\ \mathrm{m^3s/kg}$ and $\phi = 0.5$ is chosen and two FE meshes, either with 10 or 30 linear elements along the specimen are introduced. Two cases are studied. Either $P_0 = 5\mathrm{E}-5$ Pa (example 1) or $v_0^{\mathrm{D}} = 1\mathrm{E}-3$ m/s (example 2) is imposed at one end of the specimen (injection gate). Above-specified input values are shown in already multiplied forms, as described in Section 4.1. Results will be presented in terms of the original problem, although, the examples are solved exploiting the analogy.

Regarding the analogous problem described in Section 4.1, pressures P_i and P_{s} must be stated in the original problem with the correspondence to Θ_i and Θ_{s}. For the sake of simplicity, the notation c and c_0 from the analogy is kept in the original problem and no particular term is introduced for an analogue of the specific heat. Since examples with negative P_i and zero P_{s} have bad numerical properties, $P_i = 0$ is stated and the resulting $P(\mathrm{x})$ is reduced by P_{s}. Such a change is acceptable, since the constant pressure field does not influence the velocity results. Clearly, when P_0 has to be imposed, it must be imposed $P_0 + P_{\mathrm{s}}$ instead.

The influence of c_0 on the numerical filling time, T^{N}, is examined and the comparison of T^{N} with the analytical filling time, T^{A}, is provided in examples 1 and 2. T^{A} can be calculated either from the free boundary condition or from the condition

$$\int_0^{T^{\mathrm{A}}} v_{\mathrm{in}}^{\mathrm{D}}(t)\,\mathrm{d}t = D\phi,$$

where $v_{\mathrm{in}}^{\mathrm{D}}(t)$ is the Darcean velocity at the injection gate. Let us adopt the former possibility and introduce (6) into the free boundary condition. One obtains:

$$\frac{\mathrm{d}}{\mathrm{d}t}(L(t)) = \frac{v_{\mathrm{fr}}^{\mathrm{D}}}{\phi},$$

where $v_{\mathrm{fr}}^{\mathrm{D}}$ is the Darcean velocity at the "saturated region-front region" interface. It holds

$$v_{\mathrm{fr}}^{\mathrm{D}} = \frac{\mathrm{K}}{\mu}\frac{P_0}{L(t)} \quad \text{or} \quad v_{\mathrm{fr}}^{\mathrm{D}} = v_0^{\mathrm{D}}$$

and thus the saturated lengths are

$$L(t) = \alpha\sqrt{t} \text{ with } \alpha = \sqrt{\frac{2\mathrm{K}P_0}{\mu\phi}} \quad \text{or} \quad L(t) = \frac{v_0^{\mathrm{D}}}{\phi}t \tag{9}$$

in example 1 or 2, respectively. Consequently the analytical filling time is

$$T^{\mathrm{A},1} = \frac{\mu\phi D^2}{2\mathrm{K}P_0} = 18\ \mathrm{s} \quad \text{and}$$
$$T^{\mathrm{A},2} = \frac{D\phi}{v_0^{\mathrm{D}}} = 150\ \mathrm{s}, \tag{10}$$

where superscripts 1 and 2 relate to examples 1 and 2, respectively. It may be reminded the well-known fact that the filling time depends on the permeability only in example 1 and that the filling-time dependence on the total length (or more generally on the corresponding saturated length) is quadratic (linear) in example 1 (example 2).

The ANSYS default convergence criteria and automatic time step incrementation were invoked in the calculation, a restriction on a large pressure variation between the time substeps was ensured by relatively small maximum time increments, 0.05 and 0.5 s, in examples 1 and 2, respectively. When the specimen is fully saturated, i.e. at the exact numerical filling time, the problem with central difference algorithm in the time integration cannot converge, thus from the numerical results one can only extract the last "convergent time", lesser than the exact numerical filling time. Moreover, a filling-time error resulting from the nu-

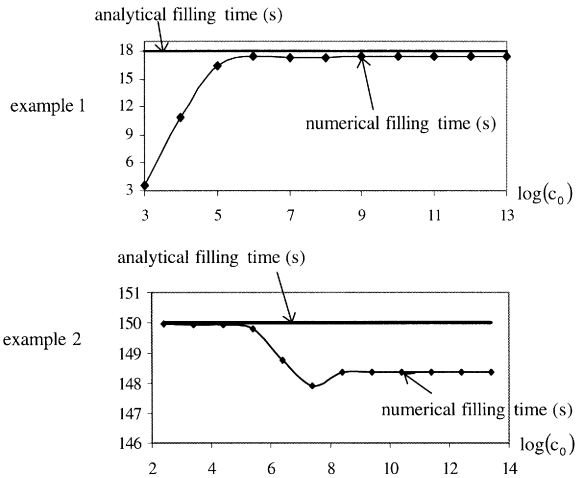

Fig. 5. Analytical filling time and the dependence of the numerical filling time on log (c_0) in examples 1 and 2.

merical errors in the time integration contributes to the total error.

The dependence of the numerical filling time on log (c_0) is plotted and compared with the analytical filling time for the two examples in Fig. 5. Several values of c_0 were used for this purpose; in example 1: c_0 (Pa^{-1}) = {1E3, 1E4, ..., 1E13}, P_s (Pa) = {5E − 4, 5E − 5, ..., 5E − 14} and l calculated using (8) for the last stage of the resin velocity is l (m) = {6E0, 6E − 1, ..., 6E − 10}. In example 2: c_0 (Pa^{-1}) = {2.5E2, 2.5E3, ..., 2.5E13}, P_s (Pa) = {2E − 3, 2E − 4, ..., 2E − 14} and l (which is now constant) is l (m) = {1E2, 1E1, ..., 1E − 9}. In both examples low c_0 values, yielding l larger than D, are inappropriate. Moreover, in these cases in example 1 the imposed value P_0 is close to or even lower than P_s.

Very good results are obtained for higher c_0, where values of the numerical filling time stabilize at 17.392 and 148.375s with errors 3.4 and 1.1%, respectively. Results in example 1 exhibit larger errors and they are also more mesh sensitive than the ones in example 2. However, until the resin front reaches the end of the specimen, the numerical front progression shows very good coincidence with the analytical predictions, as it is shown later on in this section and again in Section 4.3. It must be stressed that in ABAQUS, example 1 has very bad convergence properties and the stabilized time in example 2 (for 30 linear elements) is 115s. It is thus seen that the backward difference algorithm in the time integration is inappropriate and the results cannot be utilized in these cases. One can verify that the stabilized time for example 2 in ANSYS is 133s for $\beta = 1$ and 143s for $\beta = 3/4$.

The front region in example 1 is plotted in Fig. 6. It is seen how the sharpness changes with increasing c_0, but it is also seen that the parabolic shape used in derivation of (8) is not very appropriate. This does not cause any problem, since Eq. (8) is only used to get some c_0 estimates. The numerical saturated length, plotted in Fig. 6, exhibits for c_0 = 1E8 Pa^{-1} error 1%. The front region in example 2 is shown in Fig. 7, two saturated lengths show excellent coincidence with (9); errors 0.03 and 0.01% for c_0 = 2.5E8 (Pa^{-1}).

It can be concluded, that the range of acceptable c_0 is very large, thus the results are generally stable. Small error in the filling time is not important, since the coincidence of the analytical and numerical progression of the resin front is very good.

The main advantage of the proposed approach with respect to the FE/CV and non-conforming FE approaches is that the FE code ANSYS can be used in the RTM filling-phase simulation, bringing:

- Powerful postprocessor allowing good visualization of the resin velocities and of the exact progression of the resin front.
- Possibility of studying high variety of mold shapes, in other words, plane, shell, layered plane or layered shell as well as brick elements can be used in the corresponding FE model.

Disadvantages of the proposed approach with respect to the approaches mentioned above are:

- Slow convergence, however, ANSYS "birth" and "death" features (activating and disactivating of some elements) could be used in reducing the computational time, [7].
- Difficult end-analysis criteria.
- Necessity of c_0 estimate.
- Complicated introduction of the temperature influence, which could be only done in an uncoupled formulation.

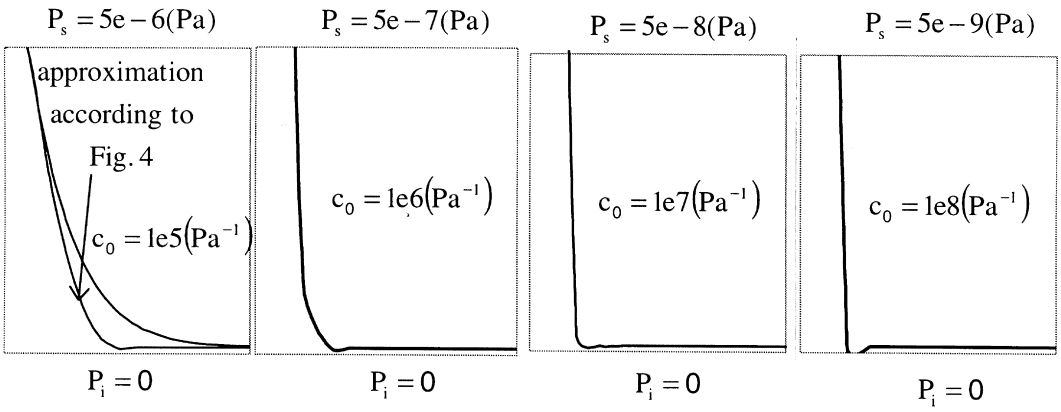

Fig. 6. The front region in example 1 for c_0 (Pa^{-1}) = {1E5, 1E6, 1E7, 1E8}, time is equal to 8.8s and the plotted part of the specimen is within [0.19 m, 0.3 m].

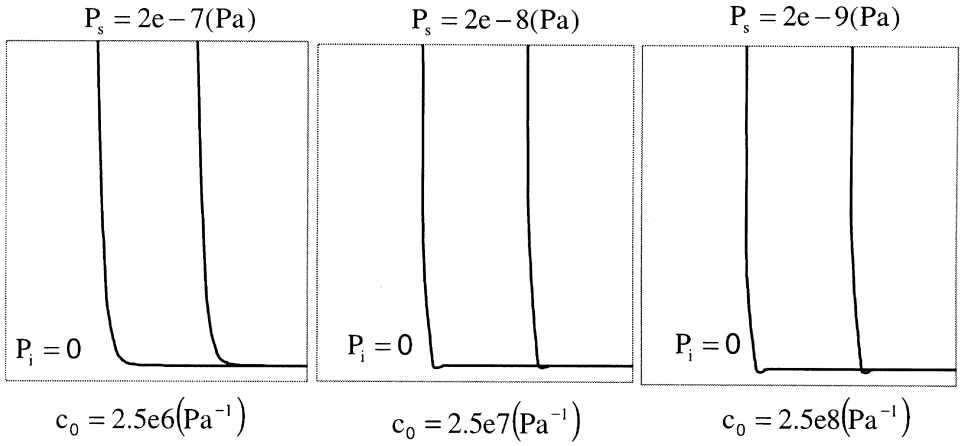

Fig. 7. The front region in example 2 for c_0 (Pa^{-1}) = {2.5E6, 2.5E7, 2.5E8}, time is equal to 50 and 100s and the full specimen is plotted.

4.3. Comparing examples and orthotropic preforms

In order to justify the reliability of the proposed approach to the macro-level analysis, two examples described in Ref. [4], whose results are compared there with experimental measurements, are examined. In addition, front progression in orthotropic preforms is compared with theoretical predictions.

As in Ref. [4] a plane rectangular mold (example 3) and the same mold but with obstacles (example 4) are assumed. The mold shape (characteristic dimensions are 1 and 0.5 m) and the FE mesh is shown in Fig. 8, linear quadrilateral elements are plotted there, since for them faster convergence is obtained. The other input values are: $\phi = 0.89$ and $\mathbf{K}/\mu = 3.41\text{E}-8$ m^3s/kg. The multiplication (see Section 4.1) with $m = 8$ is adopted and a constant flow rate at the injection gate is applied; sources $\tilde{v}_0 = 3.14\text{E}-3$ m^2/s and $\tilde{v}_0 = 3.2\text{E}-3$ m^2/s (in examples 3 and 4, respectively) are uniformly distributed in normal direction along the length of the injection gate, modeled as a ring with radius 0.01 m.

In example 3 three values of c_0 (10^{-8} Pa^{-1}) = {71.56E2, 71.56E3, 71.56E4} are tested, giving l (m) = {9.5E−3, 9.5E−4, 9.5E−5} around the gate and l (m) = {7.6E−2, 7.6E−3, 7.6E−4} in the right hand side region, where (after the left hand side of the mold is filled) the resin velocity stabilizes around the value 3.14E−3/0.5 = 6.28E−3 (m/s). Isobaric curves of $P_s = 1.25\text{E}-4$ (10^8 Pa) and $P_s/2 = 0.625\text{E}-4$ (10^8 Pa) are plotted for $c_0 = 71.56\text{E}2$ (10^{-8} Pa^{-1}) in Fig. 9. Non-sharpness of the resin front illustrates that this c_0 estimate is very low. The other two c_0 values yield very good results, see Fig. 10. Now the isobars of P_s and $P_s/2$ would be indistinguishable, thus only isobars of $P_s = 1.25\text{E}-6$ (10^8 Pa) are plotted. The isobars are not smooth, as they are affected by the linear approximation over the elements, within which still a part of the area corresponds to a constant P_i. The isobaric curves for $P(\mathbf{x}) + P_s$, plotted at $t = 105$ s in Fig. 10,

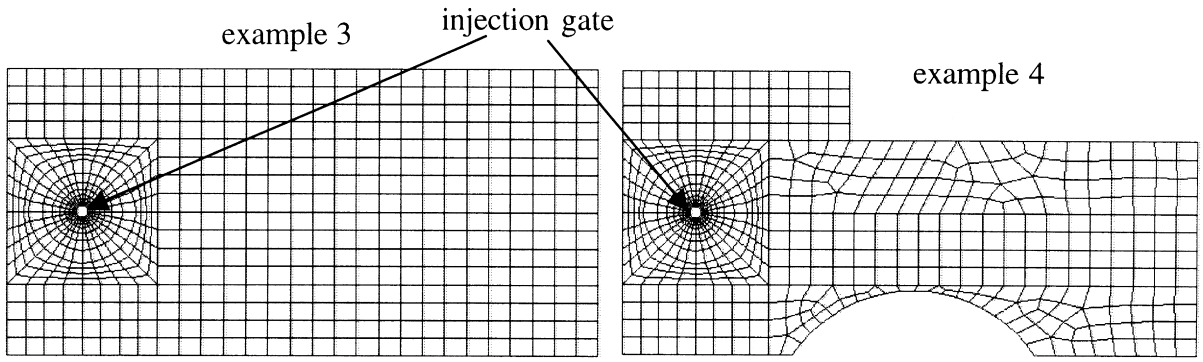

Fig. 8. FE mesh used in example 3 and 4.

are not affected by this fact and they are smooth. For the sake of comparison, the resin front is drawn in Figs. 9 and 10 at the same times as in Ref. [4]. In addition, the numerical saturated area ($c_0 = 71.56E4$ (10^{-8} Pa^{-1})) is compared in Fig. 11 with the analytical prediction. It is seen that the coincidence is very good.

An orthotropic preform with the ratio of the principal permeabilities $K_{22}/K_{11} = 2$ is studied, as in Ref. [4]. In this case the resin front as well as the isobaric curves form ellipsoids with the ratio of the principal axes equal to $\sqrt{2}$ [2,24,25] (see Fig. 12).

4.4. Multiple-layer preforms

As already mentioned in Section 2, the macro-level problem can be formulated in a layered-shell type domain. Since typical composites are very thin, one more homogenization step could be performed in the thickness direction yielding *a thickness-homogenized permeability* $^{H}\mathbf{K}$. Consequently, the macro-level problem may be defined on a two-dimensional surface, reducing significantly the memory and computational time requirements. It should be emphasized that the analytical solution of $^{H}\mathbf{K}$ on a fully saturated layered basic cell (with homogeneous layers), under periodicity boundary conditions results in $^{H}\mathbf{K} = {}^{A}\mathbf{K}$, where $^{A}\mathbf{K}$ is *the thickness-averaged permeability*.

Only recently (see [14,15]) detailed analytical studies of the problem of multi-layer preforms have been presented. The thickness-homogenized permeability is introduced in Refs. [14,15] as a function of a saturated length (notation $^{HR}\mathbf{K}$ will be used in this section), which brings several complications. In addition, in Ref. [16] the difference between the unsaturated ($^{HR}\mathbf{K}$) and saturated ($^{A}\mathbf{K}$) in-plane permeability is justified experimentally.

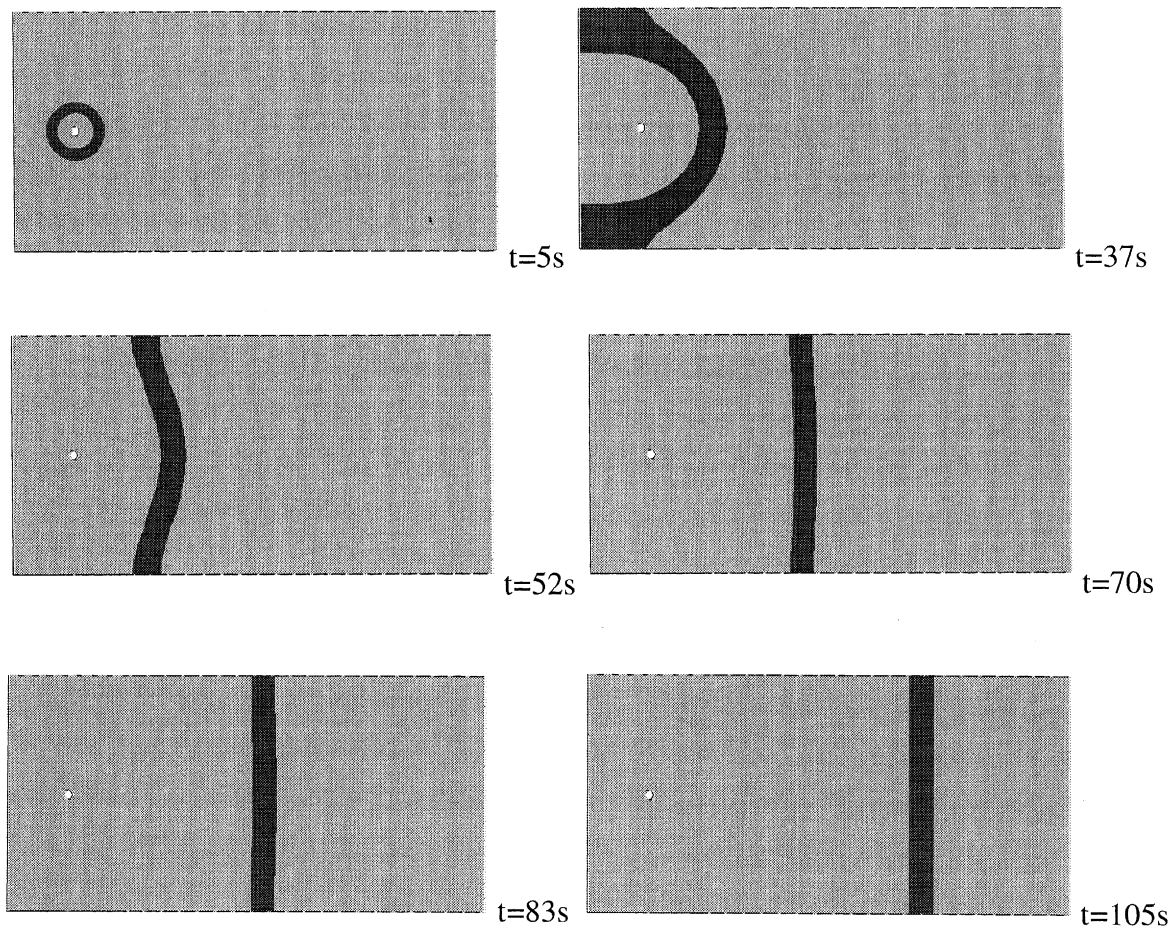

Fig. 9. Example 3 with c_0 = 71.56E2 (10^{-8} Pa^{-1}), isobaric curves for P_s = 1.25E−4 (10^8 Pa) and $P_s/2$ = 0.625E−4 (10^8 Pa) are plotted.

In this section new aspects are introduced into the study of layered specimens and the calculation of non-uniform front characteristics is proposed differently than in Refs. [14,15]. The correctness of ${}^{\mathrm{H}}\mathbf{K} = {}^{\mathrm{A}}\mathbf{K}$ is justified in the sense, that if theoretical predictions of the flow front are necessary, ${}^{\mathrm{A}}\mathbf{K}$ and characteristics of the non-uniformity calculations, using the approach proposed in this section are sufficient. In a sequel, it is not necessary to distinguish the unsaturated and saturated permeability and the dependence of the thickness-homogenized permeability on the saturated length is removed. The proposed approach is not in contradiction with the works [14–16]; it presents a different concept in the solution of the problem.

In order to properly understand the resin flow in layered specimens, the approach to the macro-level

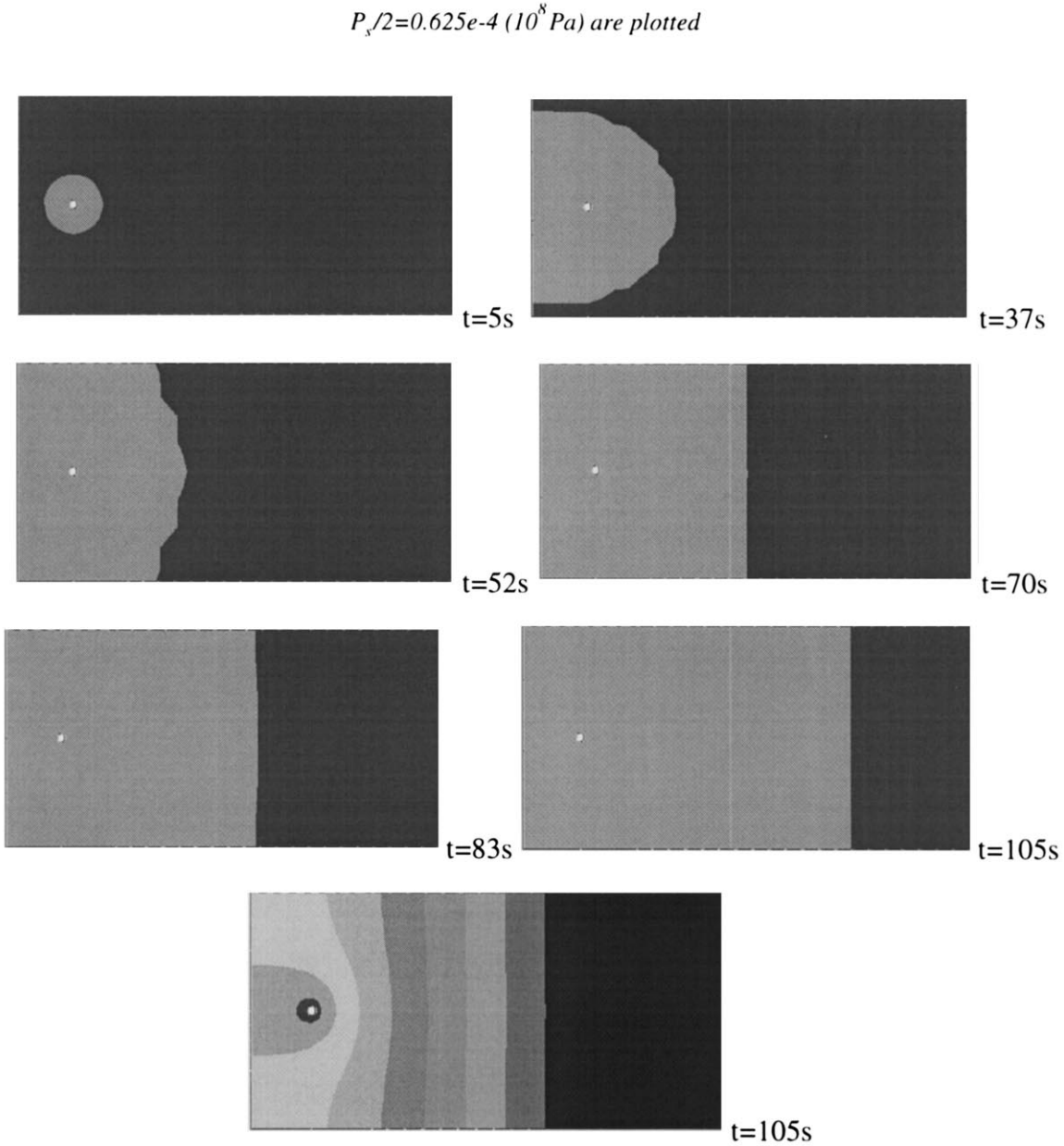

Fig. 10. Example 3 with c_0 = 71.56E4 (10^{-8} Pa^{-1}), isobaric curves for P_s = 1.25E−6 (10^8 Pa) are plotted at $t(s)$ = {5, 37, 52, 70, 83, 105} and the pressure distribution is shown at t = 105 s.

analysis proposed in Section 4.1, allowing better visualization of the results, was used. For the sake of simplicity, only two-layer medium with plane (macroscopically homogeneous) layers is studied. As in Refs. [14,15] no dependence on one of the layer direction is assumed. Initially, only a medium with layers of equal thickness is examined. The simplifying assumptions about the resin behavior from Section 2 are kept and the porosity is assumed to be constant throughout the specimen. For the sake of comparison a specimen with equal total thickness and thickness averaged permeability is included in the study (the homogenized specimen).

In detail, a specimen with total length $D = 2$ m made of two layers with equal thicknesses $h = 0.05$ m and with porosity $\phi = 0.5$ is examined. Values (after the suitable multiplication described in Section 4.1) ${}^{1}\mathrm{K}/\mu = 2$ ($\mathrm{m}^3\mathrm{s/kg}$), ${}^{\mathrm{T}}\mathrm{K}/\mu = 10$ ($\mathrm{m}^3\mathrm{s/kg}$) and ${}^{2}\mathrm{K}/\mu\,(\mathrm{m}^3\mathrm{s/kg}) = \{98, 48, 8\}$ (defining like that examples 5, 6 and 7) are introduced. ${}^{1}\mathrm{K}$, ${}^{2}\mathrm{K}$ stand for the permeability in the longitudinal direction in the two layers and ${}^{\mathrm{T}}\mathrm{K}$ denotes the transversal permeability between the layers. The thickness of the homogenized specimen is $H = 0.1$ m and ${}^{\mathrm{A}}\mathrm{K}/\mu\,(\mathrm{m}^3\mathrm{s/kg}) = \{50, 25, 5\}$ in examples 5–7, respectively. Either $P_0 = 5\mathrm{E}{-5}$ (Pa) or $v_0^{\mathrm{D}} = 1\mathrm{E} - 3$ (m/s) uniformly distributed at one end of the specimens (injection gate) was imposed, however, it was verified that in the latter case a small region around the injection gate was developed, in order to equilibrate the pressure values across the thickness. Consequently, only the former case is treated.

It is published in Refs. [14,15] and it was concluded from the performed numerical analyses:

- The transverse flow takes place only in the region close to the non-uniform front.
- The flow behind this region is not influenced by the front shape.

Thus two regions: *the homogenized region* and *the transition region*, where the transversal flow is trying to equilibrate the flow into the homogenized state (Figs. 13–15) can be distinguished in the specimen. We may remark, that Figs. 13–16 are related only to the initial part of the specimen with the length 0.3 m, for the sake of better visualization. Notation ${}^{1}P(x)$, ${}^{2}P(x)$, ${}^{\mathrm{L}}P(x)$ and ${}^{\mathrm{H}}P(x)$ is used for the pressure distribution along the specimens, superscripts 1, 2, L, H stand for layer 1, layer 2, layered and homogenized specimens, respectively, and the distribution is always assumed at the respective middle axis (Figs. 15 and 16). Moreover, notation for saturated lengths is introduced as: d in the transition region and L in the total specimen. Meaning of the superscripts is maintained, thus ${}^{1}d$, ${}^{2}d$, ${}^{\mathrm{L}}d$, ${}^{\mathrm{H}}d$ and also ${}^{1}L$, ${}^{2}L$, ${}^{\mathrm{L}}L$, ${}^{\mathrm{H}}L$ are used. In addition ${}^{\mathrm{H}}D$ stands for the length of the homogenized region (${}^{\mathrm{H}}L = {}^{\mathrm{H}}D + {}^{\mathrm{H}}d$) and $\langle d\rangle$ and $\langle L\rangle$ denote the average of ${}^{1}d$, ${}^{2}d$ or ${}^{1}L$, ${}^{2}L$, respectively. Notation is specified in Fig. 15.

The *new aspects*, that are introduced, are the following:

- In the homogenized region the flow takes place only in layers direction with constant but different velocity in each layer (Fig. 13). The pressure is independent of the transversal direction (Figs. 14 and 15), thus the ratio of the resin velocities in layer 1 (${}^{1}v^{\mathrm{H}}$) and in layer 2 (${}^{2}v^{\mathrm{H}}$) is

$$\frac{{}^{1}v^{\mathrm{H}}}{{}^{2}v^{\mathrm{H}}} = \frac{{}^{1}\mathrm{K}}{{}^{2}\mathrm{K}}. \tag{11}$$

  Eq. (11) justifies that *the homogenized region is sufficiently described by* ${}^{\mathrm{A}}\mathrm{K}$.
- The characteristics of the transition region, ${}^{\mathrm{L}}d$, ${}^{1}d$, ${}^{2}d$ and also the flow front difference, ${}^{2}d - {}^{1}d$, do not depend on the distance from the injection gate (Figs. 14 and 16), thus consequently do not depend on the transition pressure, P_{tr}, which is defined as the press-

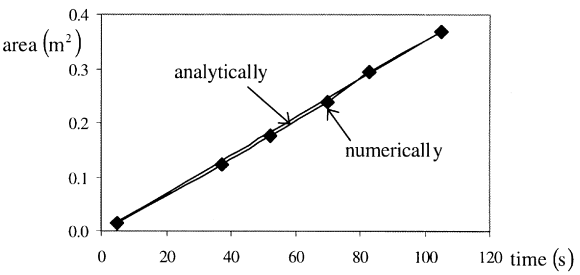

Fig. 11. Saturated area in example 3 obtained analytically and numerically $c_0 = 71.56\mathrm{E}4$ (10^{-8} Pa^{-1}).

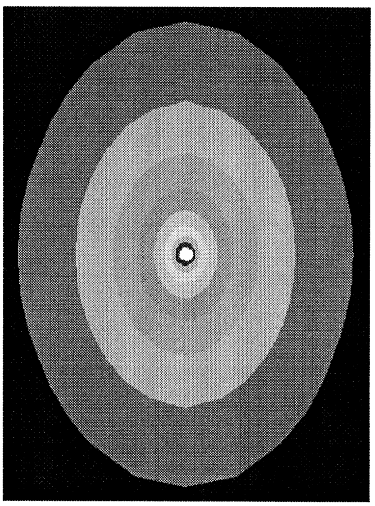

Fig. 12. Isobaric curves in orthotropic preform.

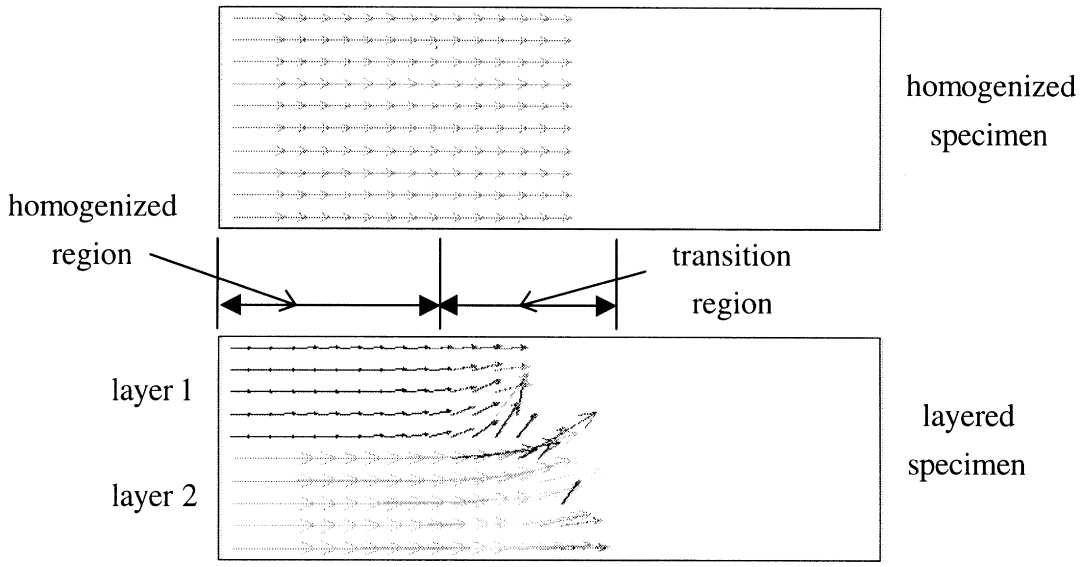

Fig. 13. Resin velocity in the homogenized and transition regions in example 7, $t = 20$ s.

ure on the interface between the two regions (Fig. 15).

- The area between ${}^{\mathrm{L}}P(x)$ and ${}^{1}P(x)$ is the same as between ${}^{2}P(x)$ and ${}^{\mathrm{L}}P(x)$ and the distribution of ${}^{1}P(x)$ and ${}^{2}P(x)$ can be approximated as piece-wise linear with different slopes in the homogenized and transition regions (Figs. 15 and 16). The slope in the homogenized region is the same for each: ${}^{1}P(x)$, ${}^{2}P(x)$ and ${}^{\mathrm{L}}P(x)$ and coincides with the slope of ${}^{\mathrm{H}}P(x)$. ${}^{\mathrm{L}}L = {}^{\mathrm{H}}L$ or ${}^{\mathrm{L}}d = {}^{\mathrm{H}}d$, while $\langle d\rangle \neq d^{\mathrm{L}}$ or equivalently $\langle L\rangle \neq L^{\mathrm{L}}$. Last two conditions show that at a specific time the total saturated volume in layered and homogenized specimens is different, i.e. the filling of the transition region in the layered specimen is firstly slower and then it equilibrates.

Simple analytical calculation of the transition region characteristics is performed in the following way. It is assumed that if the homogenous region is removed and the filling process starts from the prescribed transition pressure, P_{tr}, then it takes time, t_{tr}, to fully form the transition region. The mass balance (see [14,15]) can be written (${}^{1}\mathrm{K} < {}^{2}\mathrm{K}$) as:

$$ {}^{1}v + {}^{21}v = {}^{2}v - {}^{21}v, \tag{12}$$

where ${}^{1}v$, ${}^{2}v$ and ${}^{21}v$ are the volume rates in the transition region longitudinally in layer 1, in layer 2 and in direction from layer 2 to layer 1, respectively. Obviously:

$$ {}^{1}v(t) = {}^{1}\mathrm{K}\frac{P_{\mathrm{tr}}h}{{}^{1}d(t)\mu} \quad \text{and} \quad {}^{2}v(t) = {}^{2}\mathrm{K}\frac{P_{\mathrm{tr}}h}{{}^{2}d(t)\mu}. $$

The pressure gradient originating ${}^{21}v$ can be formulated in terms of the area of the pressure difference,

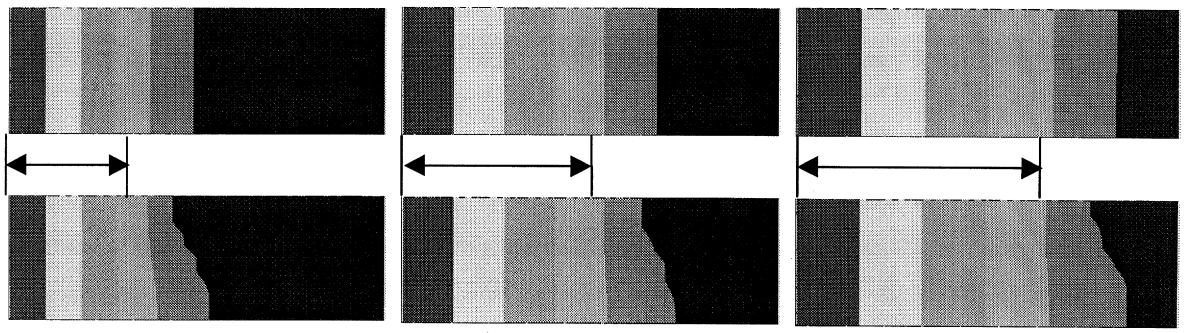

Fig. 14. Progression of pressure for $t(s) = \{20, 40, 60\}$ in example 7, the homogenized region is marked according to analytical results.

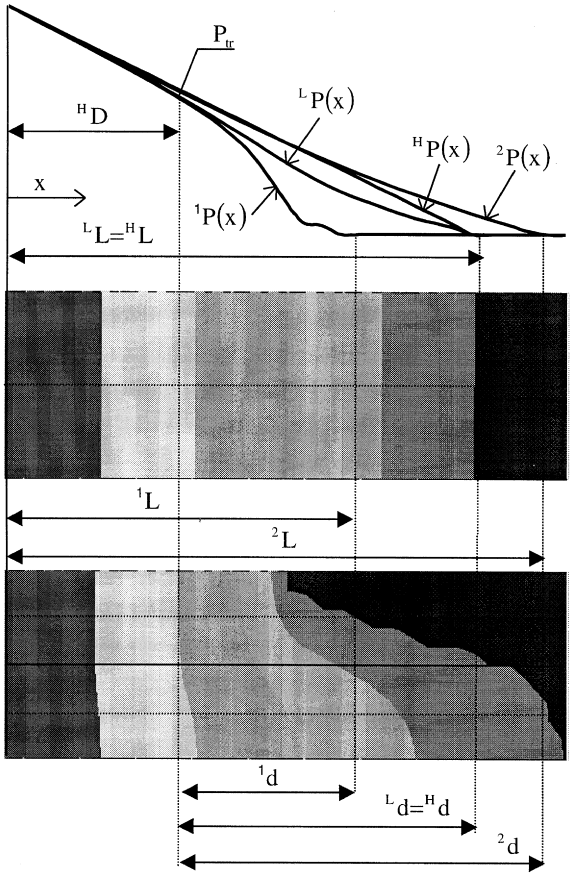

Fig. 15. Pressure distribution along the specimens and the specification of homogenized and transition regions with the introduction of notation (example 5, $t = 6.1$ s).

${}^2P(x) - {}^1P(x)$, which is $\frac{P_{tr}}{2}({}^2d(t) - {}^1d(t))$, see Fig. 17. It can be assumed, that this difference is uniformly distributed over some length (e.g. ${}^2d(t)$ or ${}^2d(t) - {}^1d(t)$), where the transverse flow takes place. However, the actual choice does not influence ${}^{21}v(t)$ and simply:

$$ {}^{21}v(t) = {}^{T}\mathrm{K}\frac{\left({}^2d(t) - {}^1d(t)\right)P_{tr}}{2\mu h}. \tag{13}$$

Only the reduced area (Fig. 17) is taken into account in the analysis in Refs. [14,15] and the flow front difference is calculated there directly from Eq. (12), where instead of ${}^1d$ and ${}^2d$, ${}^1L$ and ${}^2L$ are used. Besides of assuming ${}^1d$ and ${}^2d$ (related only to the transition region) the more important difference in the approach proposed here is, that ${}^1d$ and ${}^2d$ are assumed time dependent allowing determination of other equations, permitting the resolution of all parameters describing the non-uniform front, i.e. ${}^1d(t_{tr})$, ${}^2d(t_{tr})$ and ${}^HD$.

It is assumed that the time dependence can be expressed as in Eq. (9), now with an unknown, but time independent α. This is certainly not fully correct (compare with Eq. (12)), but it is an acceptable assumption. Total volumes of the flowing resin can be then calculated by the time integration over the interval $[0, t_{tr}]$ giving:

$$ {}^1V = {}^1\mathrm{K}\frac{2P_{tr}ht_{tr}}{{}^1d\mu}, \quad {}^2V = {}^2\mathrm{K}\frac{2P_{tr}ht_{tr}}{{}^2d\mu} \text{ and}$$

$$ {}^{21}V = \frac{\left({}^2d - {}^1d\right)P_{tr}t_{tr}{}^{T}\mathrm{K}}{3\mu h},$$

where for the sake of simplicity ${}^1d = {}^1d(t_{tr})$ and ${}^2d = {}^2d(t_{tr})$ is used. It must be satisfied:

$$ {}^1V + {}^{21}V = {}^1dh\phi \quad \text{and} \quad {}^2V - {}^{21}V = {}^2dh\phi. \tag{14}$$

Eqs. (14) and (12) with $t = t_{tr}$ substituted form the basic equations to be solved. The solution is:

$$ P_{tr}t_{tr} = \frac{3\phi\mu h^2}{4{}^{r}\mathrm{K}} \tag{15}$$

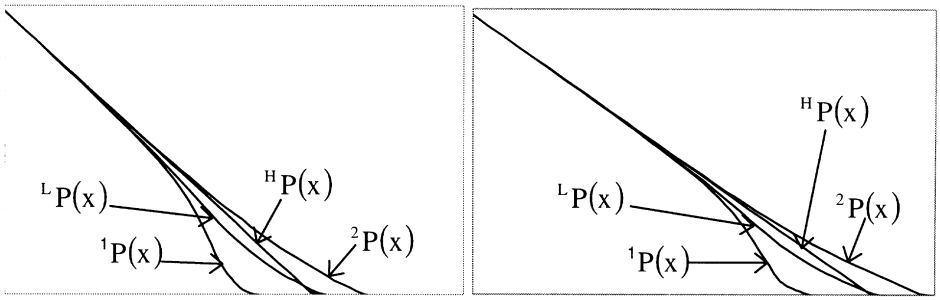

Fig. 16. Pressure distribution along the specimens in example 6, $t(s) = \{8.4, 13.5\}$.

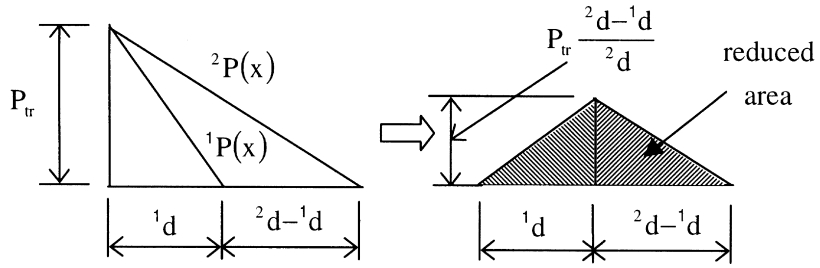

Fig. 17. Area of the pressure difference used in the determination of ^{21}v.

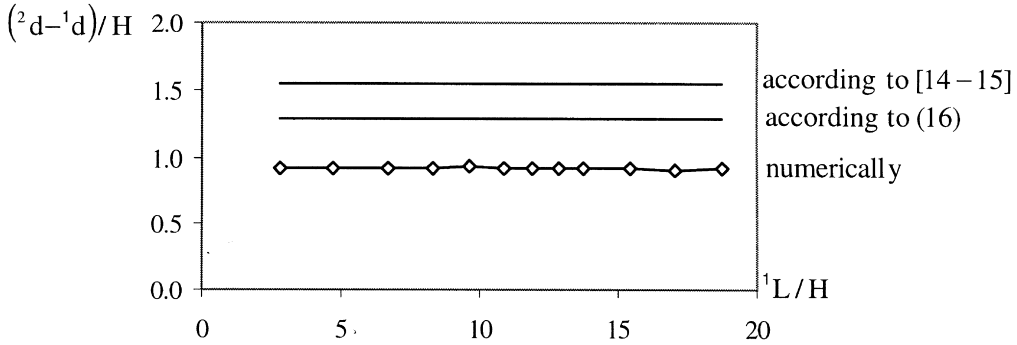

Fig. 18. Flow front difference in example 5.

and

$$^1d = \frac{h}{2\sqrt{10}}\sqrt{\frac{^2\mathrm{K} + 49^1\mathrm{K} + \sqrt{^2\mathrm{K}^2 + 98^2\mathrm{K}^1\mathrm{K} + {}^1\mathrm{K}^2}}{^T\mathrm{K}}}$$

$$^2d = \frac{5h}{2\sqrt{10}}\frac{^2\mathrm{K} + {}^1\mathrm{K} + \sqrt{^2\mathrm{K}^2 + 98^2\mathrm{K}^1\mathrm{K} + {}^1\mathrm{K}^2}}{\sqrt{^T\mathrm{K}\left(^2\mathrm{K} + 49^1\mathrm{K} + \sqrt{^2\mathrm{K}^2 + 98^2\mathrm{K}^1\mathrm{K} + {}^1\mathrm{K}^2}\right)}} \tag{16}$$

Let time t_0 be given. The non-uniform characteristics corresponding to this time can be determined in the following way. ^1d and ^2d are given by Eq. (16). Eqs. (10) and (15) yield:

$$P_{tr} = h\sqrt{\frac{3\phi\mu P_0}{4^T\mathrm{K}t_0}} \text{ and } t_{tr} = P_{tr}\frac{t_0}{P_0}. \tag{17}$$

Obviously also:

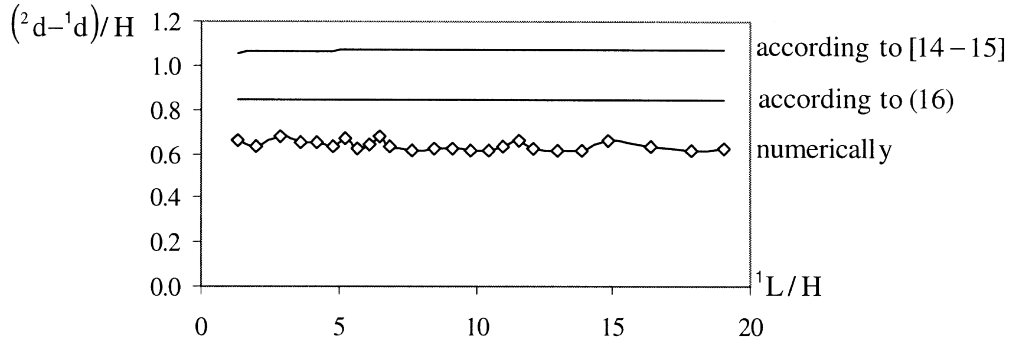

Fig. 19. Flow front difference in example 6.

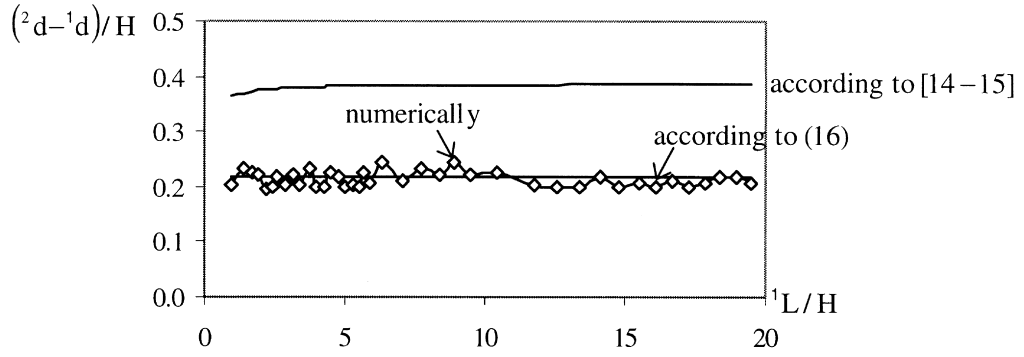

Fig. 20. Flow front difference in example 7.

$$ {}^{\mathrm{L}}L = {}^{\mathrm{H}}L = \sqrt{\frac{2\,{}^{\mathrm{A}}\mathrm{K}P_0 t_0}{\phi\mu}} \quad \text{and} $$
$$ {}^{\mathrm{H}}D = {}^{\mathrm{H}}L\left(1 - \frac{P_{\mathrm{tr}}}{P_0}\right). \tag{18} $$

It is necessary to verify, if the above-specified solution holds in the limit cases. First limit case happens when ${}^1K = {}^2K$, then from (16) ${}^1d = {}^2d$ and one can verify that

$$ \frac{{}^1d}{P_{\mathrm{tr}}} = \frac{{}^{\mathrm{H}}L}{P_0}, $$

as it should be, since ${}^{\mathrm{H}}d = {}^1d$ in this case. The above relation holds also for ${}^{\mathrm{T}}\mathrm{K} = 0$, since ${}^{\mathrm{T}}\mathrm{K}$ is not invoked there. Second limit case occurs when ${}^{\mathrm{T}}\mathrm{K} = 0$, then it can be assumed ${}^1\mathrm{K} \neq {}^2\mathrm{K}$, thus P_{tr} tends to infinity (see Eq. (17)) which corresponds to the actual state: the homogenized region is never formed. Third limit case is for ${}^{\mathrm{T}}\mathrm{K}$ tending to infinity. Then ${}^1d = {}^2d = 0$, flow is immediately equilibrated and the transition region is never formed.

Comparison of the numerical results from examples 5–7 with the derived results (16) and (18) and with the results from [14,15] is provided in the following figures. Figs. 18–20 compare the flow front difference (in a dimensionless form related to H) obtained by the above-specified three ways, plotted with respect to ${}^1L/H$. It is seen that the coincidence of Eq. (16) with the numerical results is very good; the error increases with the difference between ${}^1\mathrm{K}$ and ${}^2\mathrm{K}$. Values obtained from Refs. [14,15] reach very soon the limit $h\sqrt{(({}^2\mathrm{K} - {}^1\mathrm{K})/{}^{\mathrm{T}}\mathrm{K})}$ (already for ${}^1L \approx H$) thus discrepancies between them and Eq. (16) are caused mainly by the fact that only reduced area (Fig. 17) was introduced in Refs. [14,15]. This is also demonstrated in Fig. 21, where ${}^2d$ is plotted with respect to ${}^1d$, using Eq. (16) and according to Refs. [14,15] with ${}^1L$ and ${}^2L$ replaced by ${}^1d$ and ${}^2d$, respectively. The same comparison is done in Fig. 22, but with ${}^{\mathrm{T}}\mathrm{K}/\mu = 0.1$ ($\mathrm{m}^3\mathrm{s/kg}$) (the corresponding examples were not treated numerically) in order to show, that practically no differences between the corresponding curves are noticeable for low ${}^{\mathrm{T}}\mathrm{K}$. Since the front difference according to Eq. (16) overestimates the numerical values (especially for high difference between ${}^1\mathrm{K}$ and ${}^2\mathrm{K}$), it can be concluded, that P_{tr} proposed by (17) should be higher and ${}^{\mathrm{H}}D$ from Eq. (18) should be shorter.

Figs. 23–25 justify that the flow front progression described by ${}^{\mathrm{L}}L$ corresponds to ${}^{\mathrm{A}}\mathrm{K}$, namely the numerical ${}^{\mathrm{L}}L/H$ and ${}^{\mathrm{H}}L/H$ are compared with the theoretical prediction according to Eq. (18). The curves are plotted with respect to time and it is

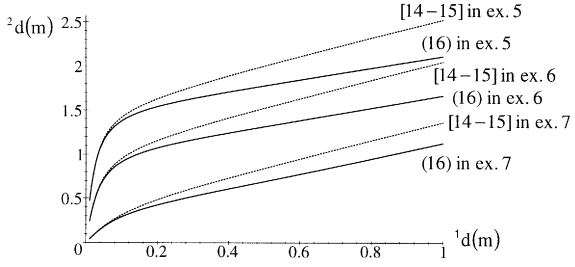

Fig. 21. Dependence of ${}^2d$ on ${}^1d$ in examples 5–7 according to Eq. (16) (full line) and [14,15] (dashed line).

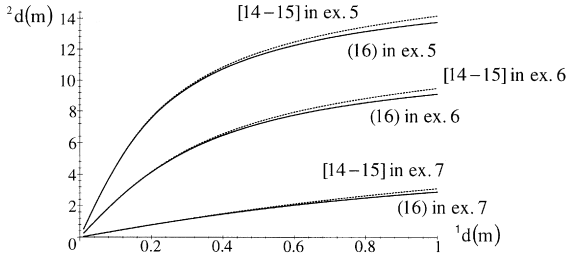

Fig. 22. Dependence of ${}^2d$ on ${}^1d$ in examples 5–7 (but with ${}^{\mathrm{T}}\mathrm{K}/ = 0.1$ $\mathrm{m}^3\mathrm{s/kg}$) according to Eq. (16) (full line) and Refs. [14,15] (dashed line).

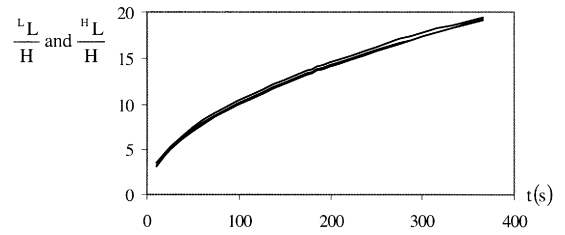

Fig. 23. Comparison of the numerical and analytical (according to Eq. (18)) ${}^{\mathrm{L}}L/H$ and ${}^{\mathrm{H}}L/H$, plotted with respect to time (in example 5).

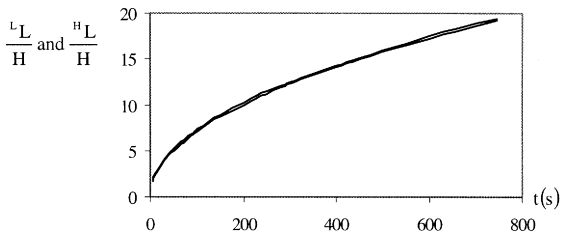

Fig. 24. Comparison of the numerical and analytical (according to Eq. (18)) ${}^{\mathrm{L}}L/H$ and ${}^{\mathrm{H}}L/H$, plotted with respect to time (in example 6).

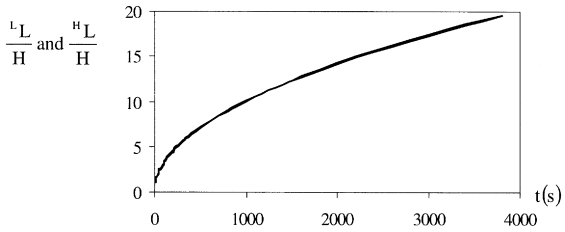

Fig. 25. Comparison of the numerical and analytical (according to Eq. (18)) ${}^{\mathrm{L}}L/H$ and ${}^{\mathrm{H}}L/H$, plotted with respect to time (in example 7).

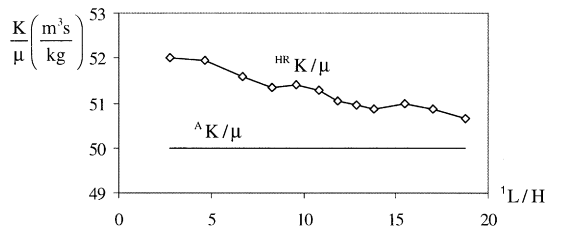

Fig. 26. Comparison of numerically obtained ${}^{\mathrm{HR}}\mathrm{K}/\mu$ with ${}^{\mathrm{A}}\mathrm{K}/\mu$, the curves are plotted with respect to ${}^{1}L/H$ in example 5.

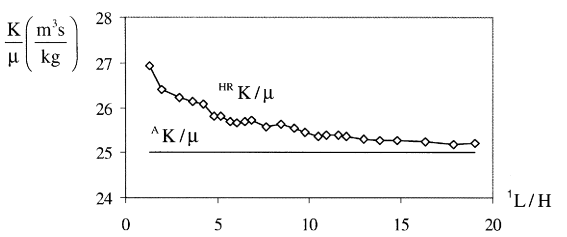

Fig. 27. Comparison of numerically obtained ${}^{\mathrm{HR}}\mathrm{K}/\mu$ with ${}^{\mathrm{A}}\mathrm{K}/\mu$, the curves are plotted with respect to ${}^{1}L/H$ in example 6.

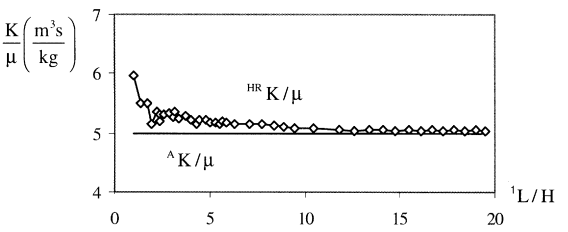

Fig. 28. Comparison of numerically obtained ${}^{\mathrm{HR}}\mathrm{K}/\mu$ with ${}^{\mathrm{A}}\mathrm{K}/\mu$, the curves are plotted with respect to ${}^{1}L/H$ in example 7.

seen that they are practically indistinguishable. Only in example 5 ${}^{\mathrm{L}}L$ slightly overestimates the result from Eq. (18).

Finally, Figs. 26–28 compare ${}^{\mathrm{A}}\mathrm{K}$ and ${}^{\mathrm{HR}}\mathrm{K}$ calculated from the numerical solution. It is seen that ${}^{\mathrm{HR}}\mathrm{K}$ differs significantly from ${}^{\mathrm{A}}\mathrm{K}$, the reason being the fact, that ${}^{\mathrm{HR}}\mathrm{K}$ is related to $\langle L\rangle$ while ${}^{\mathrm{A}}\mathrm{K}$ reflects ${}^{\mathrm{H}}L = {}^{\mathrm{L}}L$ (${}^{\mathrm{L}}L \neq \langle L\rangle$ as already emphasized).

It can be concluded that ${}^{\mathrm{A}}\mathrm{K}$ sufficiently describes the theoretical prediction of the resin front position in layered preforms. The front position (${}^{\mathrm{L}}L$) can be calculated from Eq. (18) and the non-uniform characteristics (${}^{1}d$, ${}^{2}d$ and ${}^{\mathrm{H}}D$) from Eqs. (16) and (18). Additionally also $\langle L\rangle$ can be determined. Thus, the approach proposed in this section brings valuable simplifications.

Neither the approach from this section nor from Refs. [14,15] can be utilized, when the most advanced front reaches the end of the specimen or a region of some other inhomogeneities.

5. Conclusion

In this paper some new aspects into the numerical simulation of the mold filling phase are introduced, namely, the utilization of general-purpose commercial FE codes, particularly ANSYS, is demonstrated. The utilization is made possible by stating an analogy between Stokes flow and incompressible elasticity and between Darcy's problem with moving boundary and

transient heat transfer problem. Several numerical results were presented and compared with the results taken from literature and with the theoretical predictions. The coincidence is very good in all the cases.

The approach to the progression of the resin front and very good visualization of the results in the macro-level analysis allowed better understanding of some particular problems. This was especially utilized in the study of multi-layer preforms. The usage of the thickness-averaged permeability was justified and the calculation of parameters describing the non-uniformity of the flow front was demonstrated.

Regarding possible accounting for more general resin properties, the following can be stated. Introduction of the compressibility may not cause big problems. Accounting for lower viscosities would mainly affect the micro-level problem, namely Navier–Stokes flow would have to be solved on a basic cell. Then the permeability tensor would depend non-linearly on the applied macroload as well as on the viscosity. It is questionable, if such more correct results would equilibrate the disadvantages resulting form the non-linearity of the permeability tensor. Other improvements would account for higher Reynolds number flows, influencing especially the macro-level problem, namely Forchheimer's law would have to be introduced instead of Darcy's law.

References

[1] Wocke C, van der Westhuizen J. RTM: Mould fill simulation using ABAQUS standard. In: Proc. of SA Finite Element Conference, FEMSA'95. 1995. pp. 741–55.

[2] Bruschke MV, Advani SG. A finite element/control volume approach to mold filling in anisotropic porous media. Polymer Composites 1990;11:291–304.

[3] Liu D, Bickerton S, Advani SG. Modeling and simulation of RTM: gate control, venting, and dry spot prediction. Composites 1996;27A:135–41.

[4] Trochu F, Gauvin R, Gao D-M. Numerical analysis of the resin transfer molding process by the finite element method. Advances in Polymer Technology 1993;12:329–42.

[5] ANSYS analysis guides, 1st ed., Swanson Analysis Systems IP, version 5.3, 1997.

[6] ANSYS commands reference, 7th ed., Swanson Analysis Systems IP, version 5.3, 1997.

[7] ANSYS theory reference, 7th ed., Swanson Analysis Systems IP, version 5.3, 1997.

[8] ABAQUS standard user's manual, I, Hibbitt, Karlsson and Sorensen, version 5.6, 1998.

[9] Abaqus/standard user's manual, II, Hibbitt, Karlsson and Sorensen, version 5.6, 1998.

[10] Abaqus/standard theory manual, Hibbitt, Karlsson and Sorensen, version 5.6, 1998.

[11] Papathanasiou TD. A structure oriented micromechanical model for viscous flow through square arrays of fibre clusters. Composites Science and Technology 1996;56:1055–69.

[12] Chang W. Modeling and numerical analysis of composite manufacturing processes, Ph.d. dissertation, The University of Michigan, 1993.

[13] Chui WK, Glimm J, Tangerman FM, Jardine AP, Madsen JS, Donnellan TM, Leek R. Case study from industry. SIAM Review 1997;39:714–27.

[14] Bruschke MV, Luce TL, Advani SG. Effective in-plane permeability of multilayered RTM preforms. In: Proc. of 7th Tech. Conf. on Composite Materials, American Society for Composites. 1992. pp. 103–12.

[15] Calado VMC, Advani SG. Effective averaged permeability of multi-layer preforms in resin transfer molding. Composites Science and Technonogy 1996;56:519–31.

[16] Luce TL, Advani SG, Howard JG, Parnas RS. Permeability characterization. Part II: Flow behavior in multiple-layer preforms. Polymer Composites 1995;16:446–58.

[17] White FM. In: Fluid mechanics. New York: McGraw-Hill, 1994. pp. 192–242.

[18] Sanchez-Palencia E. In: Non-homogeneous media and vibration theory, Lecture Notes in Physics, 127. Berlin: Springer-Verglag, 1980. pp. 129–57.

[19] Ene HI, Polisevski D. In: Thermal flow in porous media. Dordrecht: Reidel, 1987. pp. 1–47.

[20] Kaviany M. In: Principles of heat transfer in porous media. New York: Springer-Verlag, 1995. pp. 15–8.

[21] Darcy H. Les Fontaines Publiques de la Ville de Dijon. Paris: Dalmont, 1856.

[22] Hughes TJR. In: The finite element method, Linear static and dynamic finite element analysis. Englewood Cliffs: Prentice-Hall, 1987. pp. 192–217.

[23] Bruschke MV, Advani SG. Flow of generalized Newtonian fluids across a periodic array of cylinders. Journal of Rheology 1993;37:479–98.

[24] Carslaw HS, Jaeger JC. In: Conduction of heat in solids. Oxford: Oxford Science Publications, Clarendon Press, 1959. pp. 1–49.

[25] Adams KL, Rebenfeld L. Permeability characteristics of multilayer fiber reinforcements. Part I: Experimental observations. Polymer Composites 1991;12:179–85.